Nuclei esotici: stati eccitati, reazioni e importanza astrofisica (II)

G. Colò

Livelli di particella singola dei nuclei

- Già trattata: struttura a shell.
- Nei nuclei stabili i livelli di neutrone e protone, e in particolare le rispettive energie di separazione (ultimi livelli occupati) sono “abbastanza” simili: S_n, S_p ≈ 7-8 MeV.
- Questa situazione cambia al crescere di (N-Z)/A …

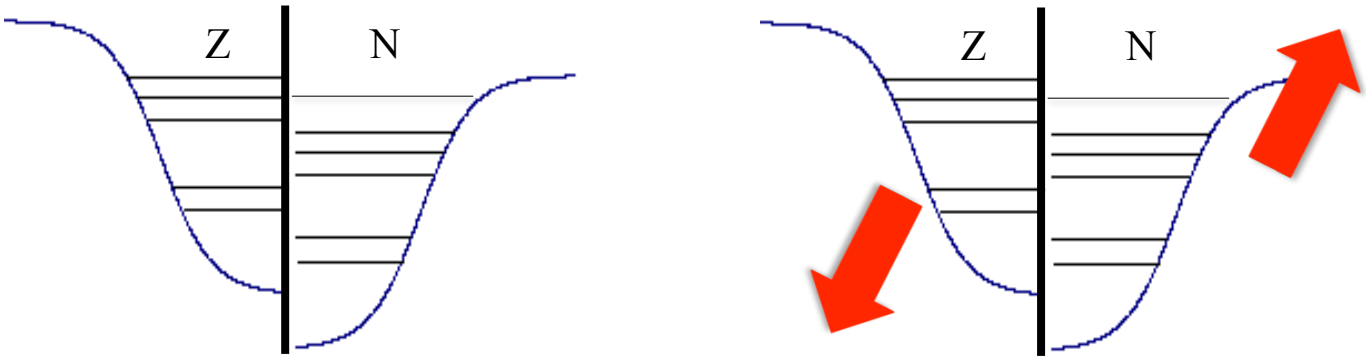

Evoluzione lontano dalla valle di stabilità

Una “regola” fondamentale: **la forza pn è notevolmente più attrattiva della forza pp o nn.** (Non è in contraddizione con le proprietà fondamentali dell’interazione forte come si può spiegare usando il principio di Pauli).

Perciò i neutroni sentono più l’attrazione con i protoni che non con gli altri neutroni. Analogamente si comportano i protoni.

In un sistema con N-Z che cresce, i neutroni occupano livelli sempre più alti e i protoni diventano più legati. Lo “squilibrio” tra neutroni e protoni aumenta, $S_p >> S_n$.

Analogamente se N-Z diminuisce, $S_n >> S_p$.

Esempi (da: I. Hamamoto/H. Sagawa)

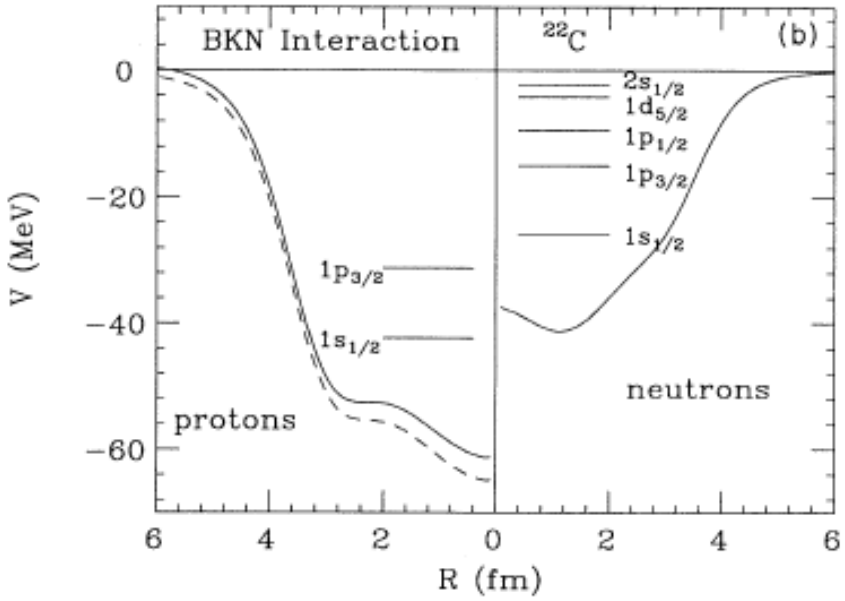

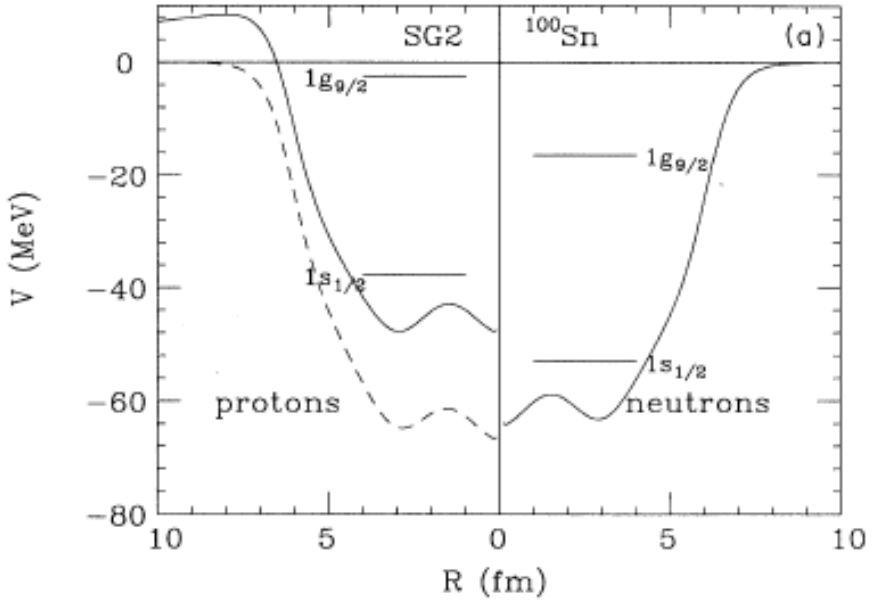

^{22}C: lecito usare “neutron-rich”
(N-Z)/A = 0.45

^{100}Sn: “proton-rich” ??
N = Z !!
“neutron-deficient”

Perché ci aspettiamo eccitazioni a bassa energia ?

In meccanica quantistica le transizioni sono favorite tra stati in cui le particelle hanno una distribuzione spaziale simile.

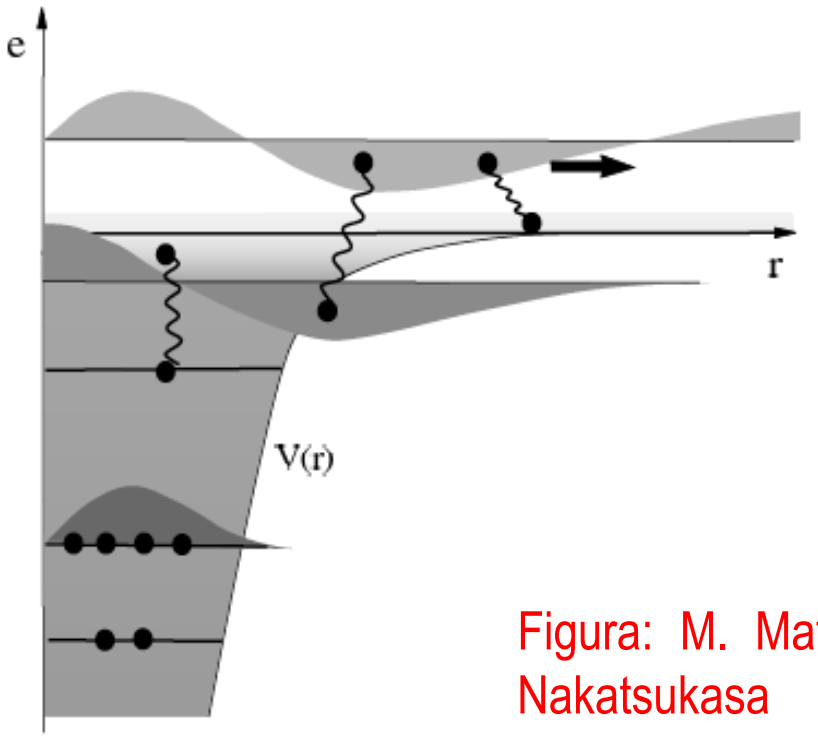

Figura: M. Matsuo e T. Nakatsukasa

Figure 2. Schematic picture depicting correlations in nuclei near the drip-line, for which correlations involving the loosely bound and unbound continuum orbits play essential roles.

Modi di vibrazione del nucleo

MONOPOLO

DIPOLO

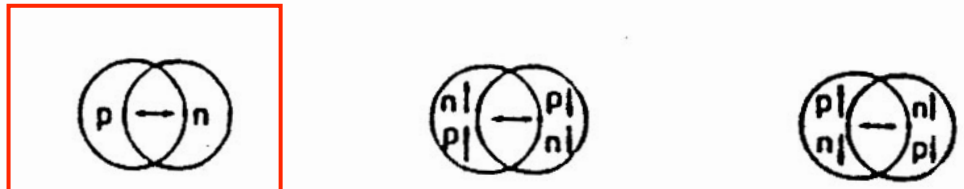

QUADRUPOLO

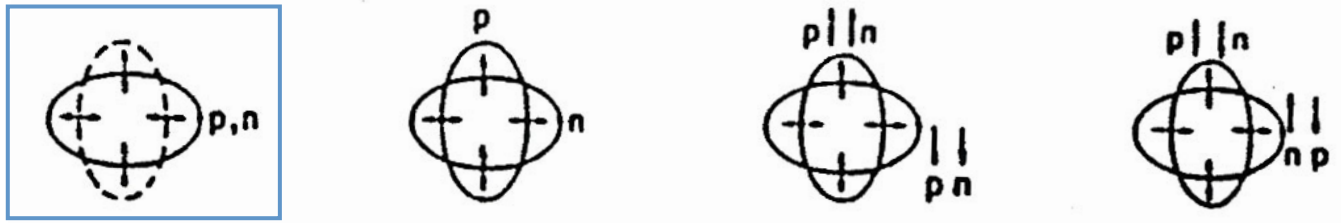

ΔT = 0
ΔS = 0

ΔT = 1
ΔS = 0

ΔT = 0
ΔS = 1

ΔT = 1
ΔS = 1

Un esempio: il dipolo “isovettoriale”

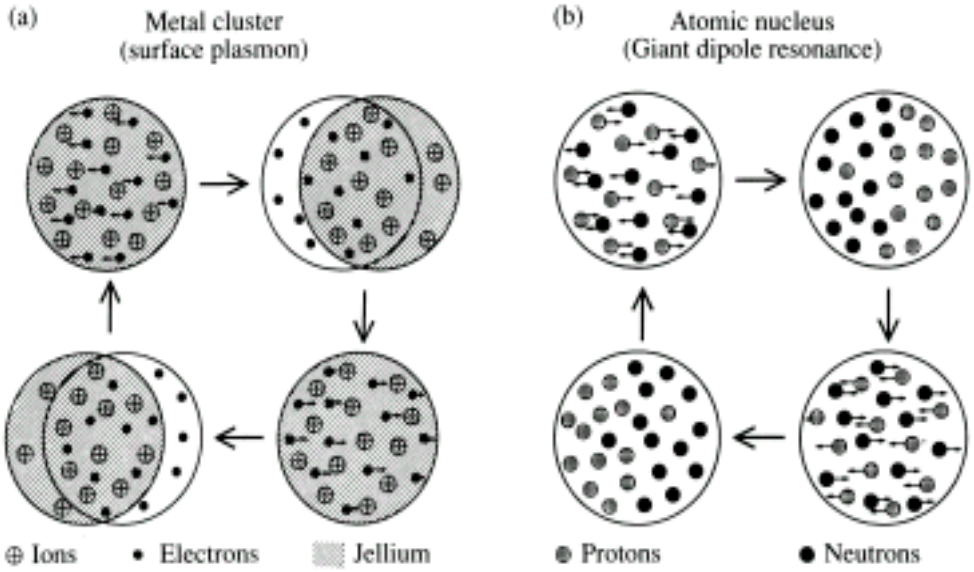

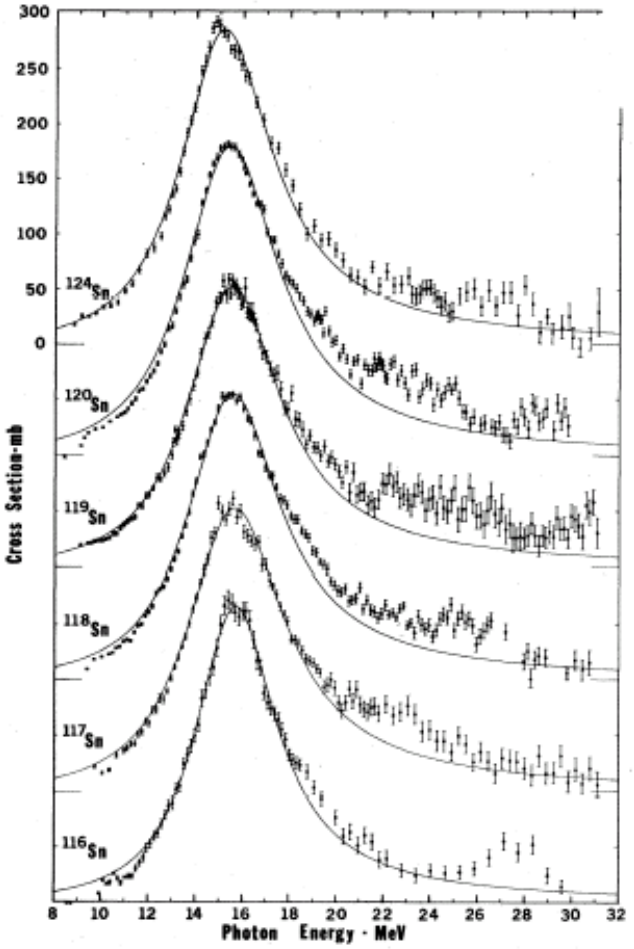

Che succede nei nuclei ricchi di neutroni o con alone ?

Eccesso neutronico

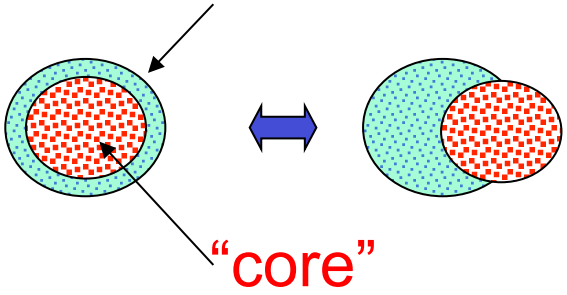

Il cosiddetto dipolo “pygmy”

O.Wieland *et al.*, PRL 102, 092502 (2009)

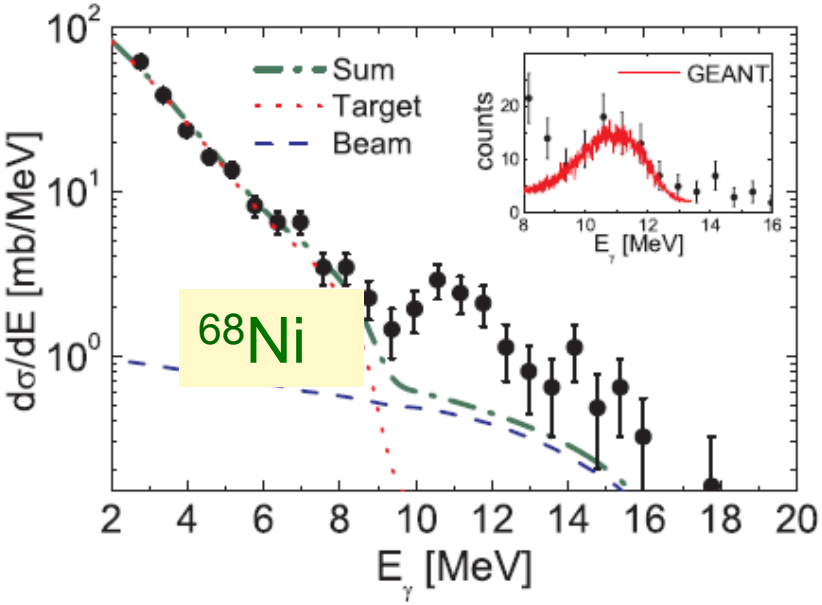

A. Klimkiewicz *et al.*, PRC 76, 051603(R) (2007).

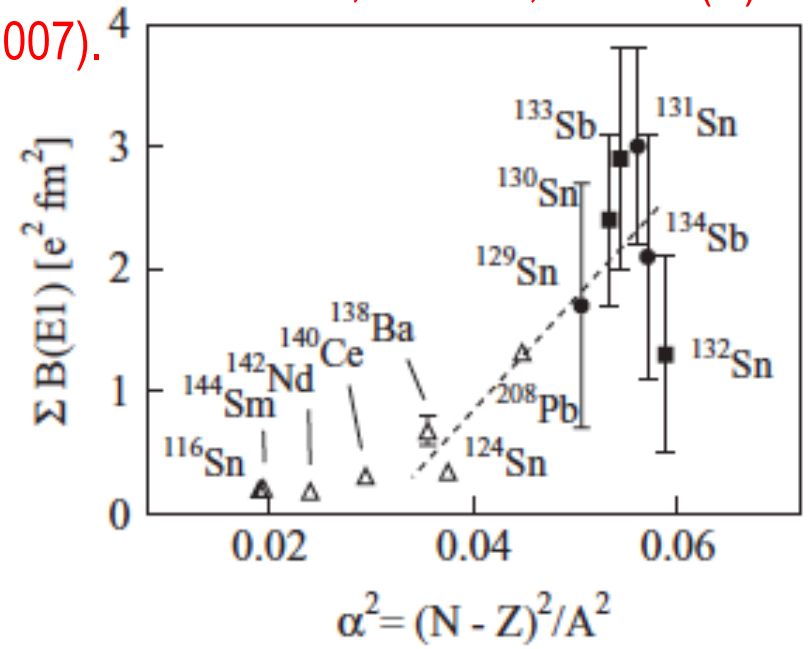

- Molti esperimenti hanno identificato stati dipolari ad energia più bassa della cosidetta “**risonanza gigante**”.
- E’ veramente una vibrazione della “**pelle**” di neutroni ?

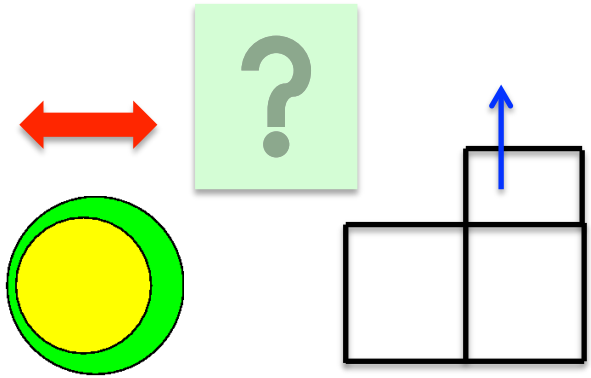

Perché la spettroscopia è interessante ?

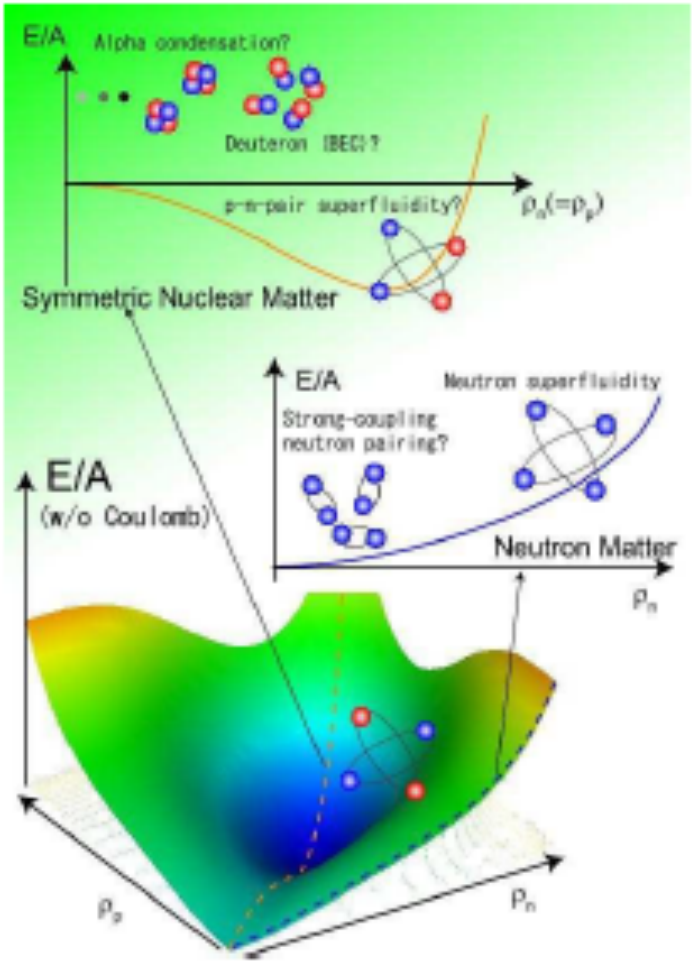

Conoscere gli stati eccitati è uno dei modi per sapere come l'energia del nucleo varia attorno allo stato fondamentale…

E, come è noto, l'Hamiltoniana nucleare non è ancora (!) conosciuta con sufficiente accuratezza.

(In particolare, ci si interroga sulla sua evoluzione quando il mezzo è a bassa densità).

Importanza astrofisica

La fisica nucleare è importante per conoscere processi quali la sintesi degli elementi, le esplosioni di supernova…
In molti di questi processi sono coinvolti nuclei esotici.

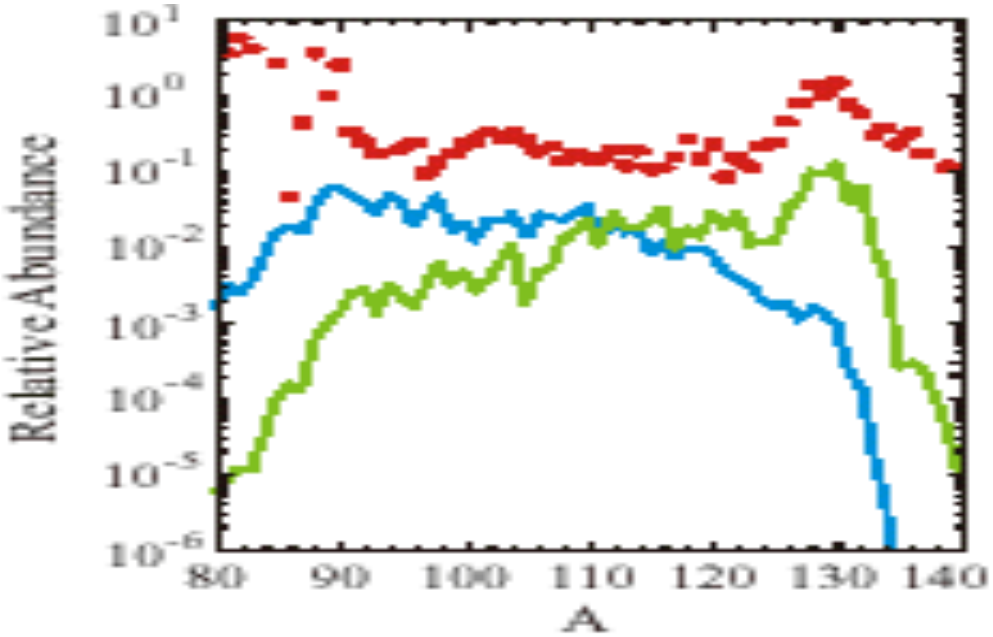

Red: empirical

Blue: no pygmy

Green: with pygmy

Stelle di neutroni

- Sistema legato di neutroni che esiste solo grazie all'attrazione gravitazionale – possibile se il numero di neutroni è molto elevato (≈10^{55}-10^{56}) !
- Osservate sotto forma di *pulsar* (J. Bell, Cambridge).
- Alcune proprietà sono note.
- Nucleo molto, molto esotico…

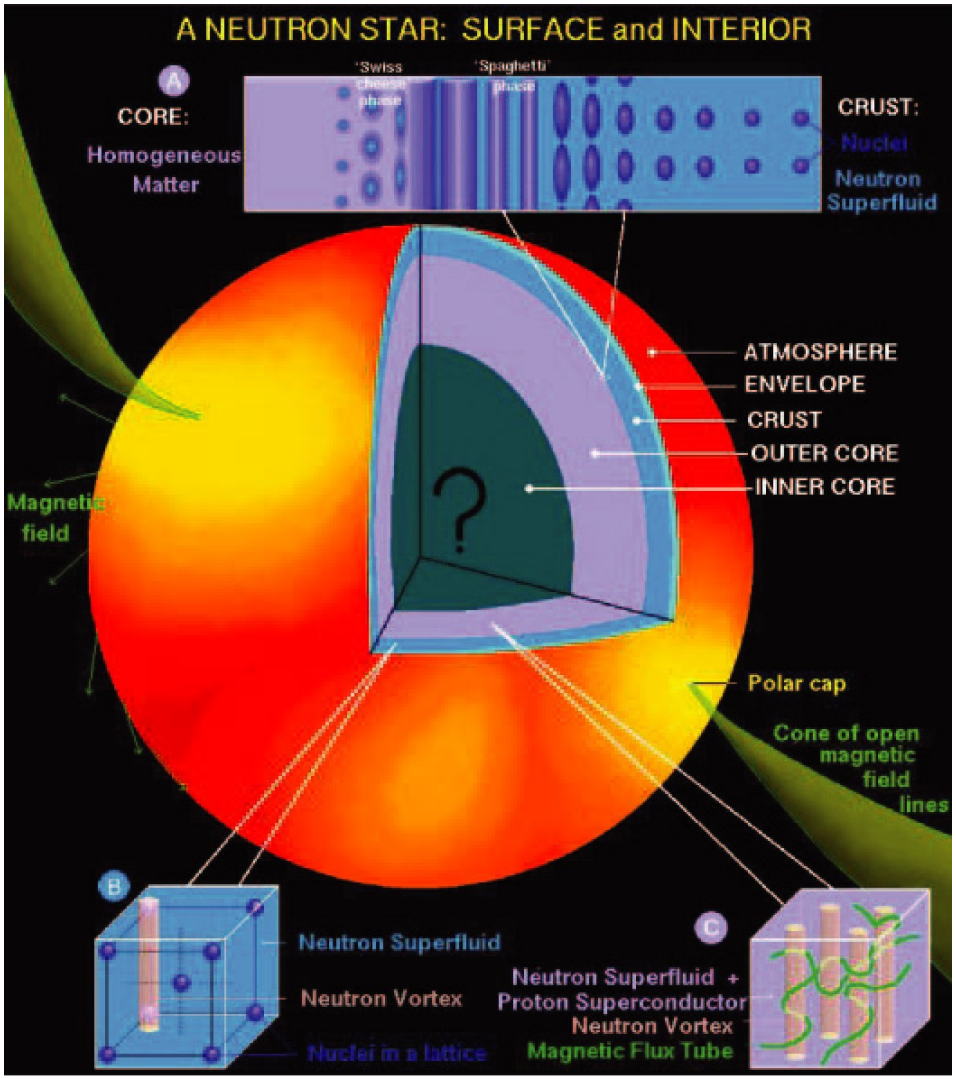

Chapter 3

SIZES AND ENERGIES OF EXOTIC NUCLEI

3.1 Introduction

The first experiments with unstable nuclear beams were designed to measure the nuclear sizes, namely the matter distribution of protons and neutrons. For stable nuclei such experiments are best accomplished with electron beams, which probe the nuclear charge (proton) distribution. Electron scattering experiments with unstable beams can only be performed in an electron-nucleus collider. Such machines are not yet available. The easiest solution is to measure the *interaction cross section* in collisions of unstable beams with a fixed target nucleus.

The interaction cross section is defined as the cross section for the change of proton and/or neutron number in the incident nucleus. To extract the *interaction radii* of the radioactive secondary beam nuclei, one has assumed that it can be expressed as [1]

$$\sigma_I(P,T) = \pi\,[R_I(P) + R_I(T)]^2 \qquad (3.1)$$

where $R_I(P)$ and $R_I(T)$ are the interaction radii of the projectile and the target nuclei, respectively. $R_I(T)$ can be obtained from σ_I in collisions between identical nuclei, while $R_I(P)$ can be obtained by measuring σ_I for different targets T [1].

The above equation assumes a separability of the projectile and target radius. This hypotheses has been tested by Tanihata and collaborators [1]. As an example, the interaction radii R_I for Li and Be isotopes have been obtained using three different targets. The results are shown in Fig. 1.

In Table 3.1 we show in the first column the interaction radii of several nuclei obtained with this technique [1]. In the last column the root mean charge radius of some nuclei obtained by electron scattering, $R^e_{\rm rms}$, are also shown. One observes that $R^e_{\rm rms}$ is almost constant for $A \geq 6$, while R_I increases with A. One can show that this difference is due to the definitions of the two radii but not due to a difference between the charge and the matter distributions. To prove it we use an eikonal calculation for the cross sections. The *rms* radius of the matter density can be determined independently of the assumed model density functions. The eikonal approximation and its use in nuclear physics is presented in Chapters 1 and 2.

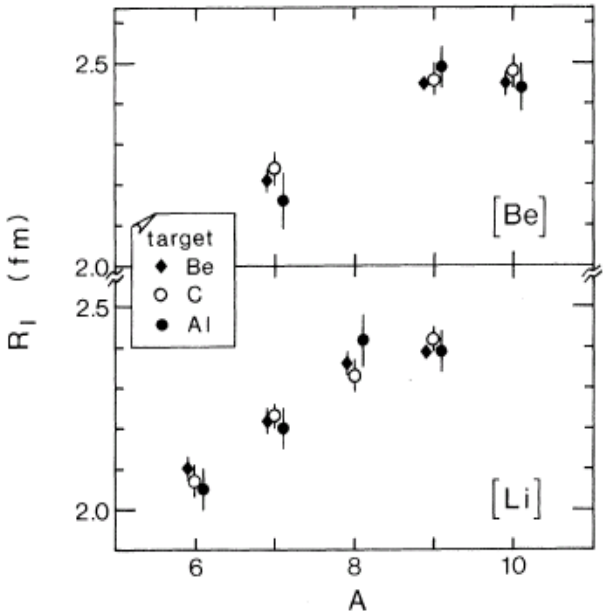

FIG. 1. R_I for Li and Be isotopes. The values obtained by three different targets agree with each other showing the separability of projectile and target R_I.

Table 3.1: cf. next page

TABLE II. Interaction nuclear radii and rms radii, in fermis.

		e scat.	Gaussian	Harmonic oscillator		
	R_I	$R^e_{\rm rms}$	$R^G_{\rm rms}$	$R^m_{\rm rms}$ [a]	$R^c_{\rm rms}$ [a]	$R^n_{\rm rms}$ [a]
^{4}He	1.41 ± 0.03	1.67 ± 0.01	1.72 ± 0.06	1.72 ± 0.06	1.72 ± 0.06	1.72 ± 0.06
^{6}He	2.18 ± 0.02		2.75 ± 0.04	2.73 ± 0.04	2.46 ± 0.04	2.87 ± 0.04
^{8}He	2.48 ± 0.03		2.70 ± 0.03	2.69 ± 0.03	2.33 ± 0.03	2.81 ± 0.03
^{6}Li	2.09 ± 0.02	2.56 ± 0.10	2.54 ± 0.03	2.54 ± 0.03	2.54 ± 0.03	2.54 ± 0.03
^{7}Li	2.23 ± 0.02	2.41 ± 0.10	2.50 ± 0.03	2.50 ± 0.03	2.43 ± 0.03	2.54 ± 0.03
^{8}Li	2.36 ± 0.02		2.51 ± 0.03	2.51 ± 0.03	2.41 ± 0.03	2.57 ± 0.03
^{9}Li	2.41 ± 0.02		2.43 ± 0.02	2.43 ± 0.02	2.30 ± 0.02	2.50 ± 0.02
^{11}Li	3.14 ± 0.16		3.27 ± 0.24	3.27 ± 0.24	3.03 ± 0.24	3.36 ± 0.24
^{7}Be	2.22 ± 0.02		2.48 ± 0.03	2.48 ± 0.03	2.52 ± 0.03	2.41 ± 0.03
^{9}Be	2.45 ± 0.01	2.52 ± 0.01	2.49 ± 0.01	2.50 ± 0.01	2.47 ± 0.01	2.53 ± 0.01
^{10}Be	2.46 ± 0.03		2.38 ± 0.02	2.39 ± 0.02	2.34 ± 0.02	2.43 ± 0.02
^{12}C	2.61 ± 0.02	2.45 ± 0.01	2.40 ± 0.02	2.43 ± 0.02	2.43 ± 0.02	2.43 ± 0.02

[a]Superscripts *m*, *c*, and *n* indicate the nuclear matter, the charge, and the neutron matter distributions, respectively.

and

$$\frac{E}{\hbar\omega} = \sum_{\Lambda=0}^{\Lambda_0} 2N_\Lambda \left(\Lambda + \frac{3}{2}\right) \cong \frac{1}{2}(\Lambda_0+2)^4 - \frac{1}{3}(\Lambda_0+2)^3 + \ldots \tag{3.35}$$

Eliminating $(\Lambda_0 + 2)$ from the above equations and retaining terms of the highest powers of $(\Lambda_0 + 2)$, we obtain

$$\frac{E}{\hbar\omega} \cong \frac{1}{2}\left(\frac{3}{2}A\right)^{4/3}. \tag{3.36}$$

Or, using 3.32 and 3.33,

$$\hbar\omega \cong 41\ A^{-1/3} \quad \text{MeV}. \tag{3.37}$$

The giant dipole resonances in nuclei are excitations with $\Delta\ell = \pm 1$ do in fact vary with the nuclear mass as $A^{-1/3}$ and are a good example of application of 3.37.

3.3 Halo nuclei

In order to show that the rms radii obtained by a comparison of reaction cross section calculations with the experimentally determined σ_I are equal, Fig. 3 shows the calculated rms charge radii and those obtained by electron-scattering experiments for stable nuclei. Even the difference between the radii of ^{6}Li and ^{7}Li because of the occupation-number difference between protons and neutrons is reproduced by the harmonic-oscillator distribution (solid line). The rms radii obtained with Gaussian distributions (which are the same for protons as for neutrons) is shown by the dashed-line.

The calculations also show that R_I represents the radius where the matter density is about 0.05 fm^{-3} for $A \geq 6$ nuclei. Now we can understand why the rms radii and R_I behave differently with A. While the rms radii stay constant, the absolute density increases with A. Therefore R_I, which represents constant density, increases with A. These interesting results are presented in figure 5(a) where the rms radii of He, Li, Be, and C isotopes are shown [7]. The curves are guides to the eyes.

We observe a great increase in the rms radii for the neutron-rich isotopes ^{6}He, ^{8}He and ^{11}Li. Thus, the addition of the neutrons to ^{4}He and ^{9}Li nuclei increase their radii considerably. This might be understood in terms of the binding energy of the outer nucleons. The large matter radii of these nuclei have lead the experimentalists to call them by "*halo nuclei*". The binding energy of the last two neutrons in ^{11}Li is equal to 315 ± 50 keV [6]. In ^{6}He it is 0.97 MeV. These are very small values and should be compared with $S_n = 6 \div 8$ MeV which is the average binding of nucleons in stable nuclei.

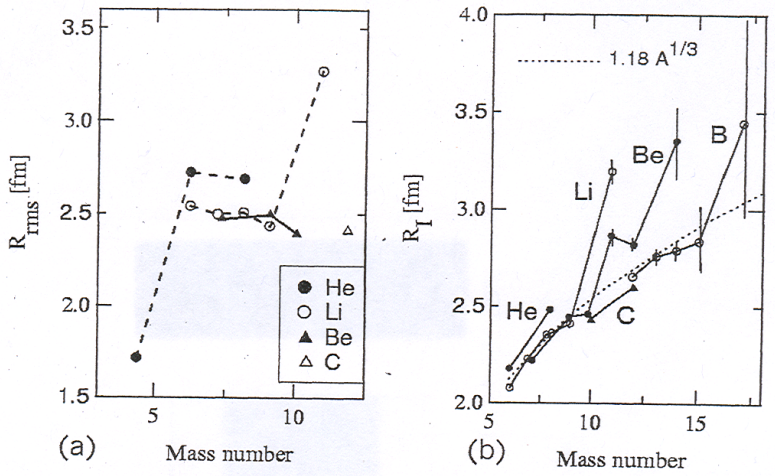

Figure 5 (a) Rms radii for the neutron-rich isotopes He, Li, Be, and C. (b) The matter density radii of several light nuclei compared to the trend $R \sim 1.18\ A^{1/3}$ fm (dashed line) for normal nuclei. The solid lines are guide to the eyes.

The wavefunction of a loosely-bound nucleon (as in the case of the deuteron) extends far beyond the nuclear potential. For large distances the wavefunction behaves as an Yukawa function,

$$R(r)/r \sim \frac{e^{-\eta r}}{r} \tag{3.38}$$

where $(\hbar\eta)^2 = 2mB$, with B equal to the binding energy and m the nucleon mass. Thus, the smaller the value of B is, the more the wavefunction extends to larger $r's$. Thus the "halo" in an exotic unstable nuclei, like ^{11}Li, is a simple manifestation of the weak binding energy of the last nucleons. What is not as trivial is to know why ^{6}He and ^{11}Li are bound while ^{5}He and ^{10}Li are not. We will continue this discussion later.

Abnormally large radii were also found for other light neutron-rich nuclei [7] as shown in figure 5(b).

The matter density radii of these nuclei do not follow the commonly observed trend $R \sim 1.18\ A^{1/3}$ fm of normal nuclei. Thus the halo seems to be a common feature of loosely-bound neutron-rich nuclei. In Table 3.3 we list the spin, parities and mass number of some light neutron-rich nuclei. The separation energy of one neutron (S_n) and of two neutrons (S_{2n}) are also shown. One observes that the two-neutron separation energies of ^{11}Li, ^{14}Be and ^{17}B are very small and are responsible for large matter radii of these nuclei, as seen in figure 5(b). A nuclear chart with the halo nuclei is shown in Figure 6.

Other evidences

• Other experiments which have been historically important, to make the character of halo nuclei evident, are: (i) momentum distributions of projectile fragments, and (ii) electromagnetic dissociation.

These are reviewed in papers e.g. by I. Tanihata.

The idea of the momentum distribution experiments is quite simple. If we hit, e.g., ^{11}Li on a C target at 800 MeV/u we can measure the transverse momentum of the fragments and we find a “double” distribution.

The component with “small width” has a Δp of about 19 MeV/c. From the uncertainity principle

$$\Delta x \sim hc/\Delta p \sim 12 \text{ fm},$$

that is, the narrow component is arising from the halo.

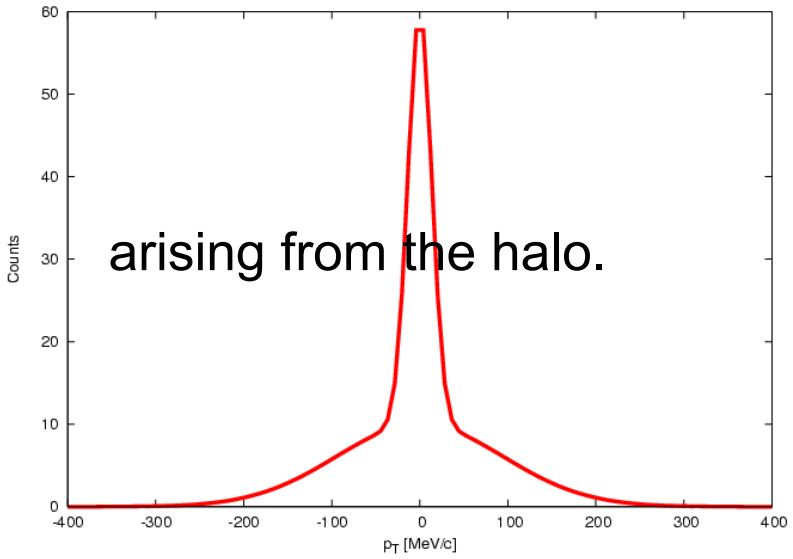

The best-fitted density distribution $\rho(r)$ for ^{11}Li is shown in Fig. 10. For the halo neutrons, 1p or 2s orbits were assumed, and the both fits gave essentially the same distribution as seen in the figure. A difference was seen in the orbital energy, which was ascribed to the centrifugal-barrier effect. It was noted here that the selection of orbital was more or less arbitrary and only the final density distribution had the practical meaning. The obtained density distribution gave the rms radii, $R_{rms}(^{11}\mathrm{Li})$ =3.1 ± 0.3 fm, and R_{rms}(2n) =4.8 ± 0.8 fm for the ^{11}Li nucleus and the halo neutrons, respectively. The size of the ^{9}Li core (R_{rms} ~2.6 fm) turned out to be slightly larger than that of the ^{9}Li nucleus (R_{rms} =2.32 ±0.02 fm), qualitatively consistent with the center-of-mass motion of ^{9}Li core in ^{11}Li.

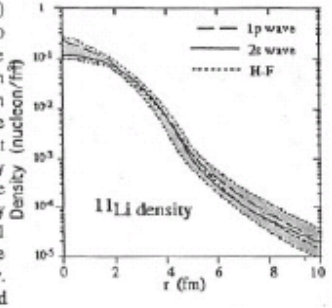

Fig. 10. Density distribution of ^{11}Li deduced from the interaction cross sections. The selection of orbitals, 1p or 1s for the halo neutrons, gave only a minor difference. The shaded area shows the fitting uncertainty. The dotted line shows the H-F model prediction constrained by the last neutron separation energy.

Functional shapes other than the one described above were also investigated: a) Single Gaussian gave no good fit to the data and was definitely inappropriate. b) Gaussian core + Yukawa tail gave also a good fit and the obtained $\rho(r)$ showed essentially the same halo tail but with a slightly higher central density.

Intensive theoretical studies have been performed to understand the structure of these halos by various authors. Bertsch, Brown and Sagawa [19] made a Hartree-Fock calculation by constraining the separation energy of the last occupied orbit. The calculated density distributions are shown in corresponding figures (Fig. 9 and Fig. 10). They show good agreement with the present semi-empirical result. An important implication of the HF calculation is that the long tail of the density distribution mainly arises from the weakly-bound last neutron.

A microscopic model of ^{11}Li was developed by Ikeda, Suzuki and their collaborators [20] by a hybrid model combining a cluster-orbital-shell model with an extended cluster model. The model gave a plausible explanation of the binding mechanism of the three-body system of ^{9}Li+n+n, and both the rms radius and the last-neutron binding energy were consistently reproduced.

4.3 Momentum distributions

Studies of projectile fragmentation at high energy (≥400 MeV/nucleon) shows that the momentum distribution of nucleons inside a projectile nucleus can be determined from the momentum distribution of the projectile fragments. Extending the method used for stripping reactions to many nucleon removal, the width of the P_t distribution* of the projectile fragment is expressed by the separation energy of last neutrons,

$$\sigma^2 = 2u\langle E_s\rangle \frac{A_F(A_P - A_F)}{A_P}, \qquad (4.5)$$

where u is the atomic mass unit and $\langle E_s\rangle$ is an average separation energy of the removed nucleons. It is essentially the same conclusion with the discussion in sec. 4.1.

The transverse momentum distributions of fragments of ^{11}Be and ^{11}Li by carbon target were firstly measured at 790 MeV/nucleon.[3] Figure 11 presents a transverse momentum distribution of (a) ^{10}Be fragment from ^{11}Be + C reaction and (b) ^{9}Li fragment from ^{11}Li + C reaction both at 800A MeV. Both of the data show a very narrow peak on top of another wider peak. The fitting of the momentum distribution by two gaussians gives the width to be σ_{narrow}=25 ± 4 MeV/c and σ_{wide}=109 ± 7 MeV/c for ^{10}Be spectrum. In ^{9}Li, σ_{narrow}= 21 ± 3 MeV/c and σ_{wide}= 80 ± 4 MeV/c. The narrow peaks indicates an existence of neutrons with extremely small momentum fluctuation as expected in the neutron halo. The σ_{wide} is consistent with the momentum fluctuations of usual nucleons.

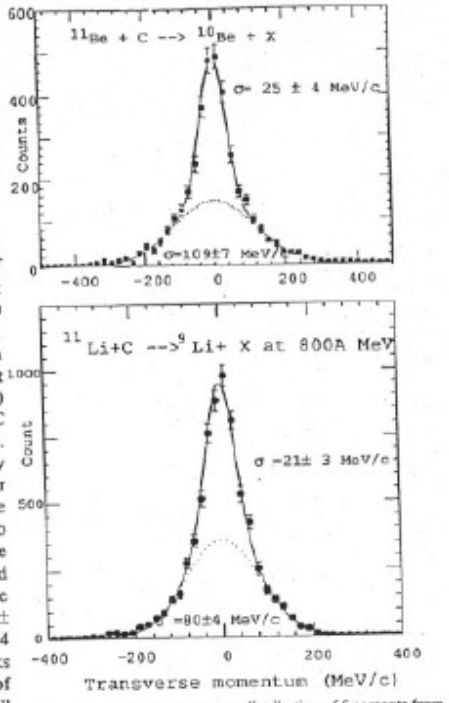

Fig. 11. Transverse momentum distribution of fragments from halo nuclei ^{11}Be and ^{11}Li

* The P_t distribution ($d\sigma/dP_t$) here is defined as,

$$\frac{d\sigma}{dP_t} = \iint \frac{d^3\sigma}{dP_x dP_y dP_{//}} dP_y dP_{//}$$, where $(P_t, P_y, P_{//})$ corresponds to the momentum vector in the Cartesian coordinate (x,y,z) with z being the direction of an incident beam.